scientific reports

Check for updates

OPEN

Widespread heat stress will become the norm in a warming Southeast Asia

Sonali Manimaran[1,2]✉, Dennis Wagenaar[1,2], Christine Nam[3], Indraneel Kasmalkar[1], Ludwig Lierhammer[4], Laurens M. Bouwer[3,5] & David Lallemant[1,2]

Southeast Asia faces growing risks from extreme heat under climate change, yet existing assessments do not fully account for physiological impacts and population-level exposure, particularly at resolutions relevant for planning. Here we present a comprehensive evaluation of future heat stress in the region by integrating three methodological innovations: physiologically relevant bio-climatic indices, spatially explicit population exposure, and sub-daily temporal resolution. Using the Universal Thermal Climate Index (UTCI) and Wet-Bulb Globe Temperature (WBGT), we assess heat stress across Southeast Asia at 22×22 km spatial and 3-hourly temporal resolution under low- and high-emissions scenarios. We combine these projections with population data to identify where and when risks are most acute. Our results show that even by the near-future (2030–2059), exposure to life-threatening extremes (UTCI > 46 °C, WBGT > 33 °C) increases sharply, by factors of 2.8–4.6 (UTCI) and 4.6–7.9 (WBGT) relative to historical levels. The number of people exposed to at least one consecutive week of extreme UTCI grows from 9 million historically to 23–28 million under RCP2.6 and RCP8.5, while extreme WBGT exposure increases from 0.1 million to 7–17 million. Continental Southeast Asia, including Myanmar, Thailand, and Cambodia, faces the most acute risks, with 6–9 hours of severe heat stress per day during peak months. By the far-future (2070–2099) under RCP8.5, exposure escalates to catastrophic levels, with up to 200 days per year of unsafe conditions and exposed populations increasing more than tenfold. Our findings show that dangerous levels of heat stress will emerge within decades, underscoring the urgency of adaptation and the benefits of strong mitigation.

Keywords Heat stress, Extreme heat, Climate change, Exposure, Southeast Asia, UTCI, WBGT

Extreme heat in Southeast Asia has increased in recent years, with heatwaves becoming more frequent, lasting longer, and exhibiting greater severity[1–3]. Although the region's predominantly tropical climate naturally produces both dry- and humid-heat extremes[4], climate change is intensifying these conditions through increases in temperature and changes in humidity, with record-breaking extremes and heatwaves occurring in the past decade[4,5]. The heatwaves of April–May 2024, for example, resulted in widespread school closures, agricultural losses, increased heat-related illnesses, and at least 40 reported fatalities[6–8]. Concurrently, Southeast Asia has undergone significant socioeconomic changes. Its population, across its 11 constituent countries, has surged from approximately 215 million in 1960 to nearly 695 million today[9]. Economic growth has averaged around 5% annually since the 1990s, and approximately 50% of residents now live in urban areas[10]. These converging trends of escalating climate hazards and rapid demographic and urban growth highlight the urgent need for robust projections of future heat stress across the region.

While research on future heat extremes in Southeast Asia is expanding, studies to date remain limited in accurately characterising human exposure to heat stress. Studies in Southeast Asia have generally projected heat extremes from temperature-based metrics[1,11–13], but temperature alone does not fully capture heat stress, as it needs to be considered in conjunction with other meteorological variables, such as humidity, wind speed and radiation, in order to comprehensively assess thermal load on the human body[14]. Compared to temperature-

[1]Earth Observatory of Singapore, Nanyang Technological University, 50 Nanyang Ave, Singapore 639798, Singapore. [2]Asian School of the Environment, Nanyang Technological University, 50 Nanyang Ave, Singapore 639798, Singapore. [3]Climate Service Center Germany (GERICS), Helmholtz-Zentrum Hereon, Fischertwiete 1, Hamburg 20095, Germany. [4]Copernicus Climate Change Service, German Weather Service (DWD), Bernhard-Nocht-Straße 76, Hamburg 20359, Germany. [5]Institute of Geography, University of Hamburg, Bundesstraße 55, Hamburg 20146, Germany. ✉email: emsonali@gmail.com

based metrics, bio-climatic indices offer a more accurate assessment of heat stress because they integrate multiple meteorological variables when computing thermal load. Some indices incorporate physiological modeling of thermoregulation[14], while others are based on empirical correlations between environmental conditions and physiological responses[15]. Despite their advantages, the applications of bio-climatic indices in Southeast Asia have been limited to historical trend analysis[16] and trend-extrapolated projections[17]. Additionally, assessing the people-centric impact of heat stress necessitates integrating population distributions within heat stress projections to identify where people actually live relative to extreme heat hazards, thereby revealing exposure hotspots rather than hazard patterns alone. While global-scale studies have applied bio-climatic indices alongside population exposure, they rely on coarse spatial projections[18–21], limiting their applicability for regional-scale planning. In contrast, some regional assessments in Southeast Asia have used finer-scale climate and population data, yet evaluate exposure only through temperature-based metrics and heatwave frequencies[11,12], overlooking the additional physiological insights provided by integrated bio-climatic indices. Moreover, the temporal resolution of existing heat stress projections fails to capture physiologically critical patterns of exposure. Most studies[1,4,5,16,19–22] use daily or monthly maxima or averages, masking diurnal patterns of daytime heat accumulation and nighttime recovery that are relevant to human thermoregulation. This coarse temporal aggregation lacks the precision needed to design effective interventions that match the actual duration and timing of dangerous heat exposure.

This study advances heat stress assessment in the region through three interconnected innovations that address these gaps. First, we compute two complementary bio-climatic indices at high-resolution (22x22km): the Wet-Bulb Globe Temperature (WBGT), which underpins occupational health standards and work–rest guidelines[15,23], and the Universal Thermal Climate Index (UTCI), which employs a dynamic human thermoregulation model to reflect physiological responses and behavioural adaptation[14,24]. Second, we integrate these with downscaled Shared Socioeconomic Pathway (SSP) population data to quantify exposure at policy-relevant scales, identifying precisely where people face the greatest risks. Third, our use of 3-hourly climate data enables detailed analysis of sub-daily heat variability, identifying dangerous peaks and inadequate recovery periods. Together, these advances provide the first comprehensive assessment of heat stress across Southeast Asia that links climatic extremes with human exposure patterns and physiological impacts, providing a new benchmark for regional climate risk assessment that can inform targeted adaptation strategies. The datasets developed in this study can also serve as foundational inputs for a wide range of follow-on studies – including epidemiological analyses of heat-related morbidity and mortality, evaluations of labour productivity losses, and socio-economic vulnerability assessments – thereby supporting research into the health, social, and economic impacts of extreme heat.

Results

We used climate projections from the REgional MOdel (REMO) regional climate model (RCM)[25,26] to compute UTCI and WBGT for the historical baseline (1976–2005), near-future (2030–2059) and far-future (2070–2099) time periods, with RCP2.6 and RCP8.5 being considered in the latter two time periods. . Computations were done on a 22×22 km grid size across Southeast Asia, at a 3-hourly temporal resolution. The results are reported according to the standard classification schemes for UTCI and WBGT (see Sect. "Methods" for details). UTCI represents the equivalent air temperature under a standardised reference condition that would produce the same physiological response as actual environmental conditions. It integrates air temperature, humidity, wind speed and radiation and is classified into ten standardised thermal stress levels[14]. WBGT combines natural wet-bulb, globe and air temperatures to quantify environmental heat load in occupational settings. It classifies conditions into six workload categories - each prescribing maximum continuous work durations and minimum rest periods under ISO 7243 guidelines[15]. The statistics reported in this section are weighted by population according to downscaled SSP population projections, in order to provide a people-centric rather than land-centric perspective on heat stress. The same population data were also used in the exposure calculations. Section "Methods" has a detailed description of the methodology used.

Heat stress in Southeast Asia will intensify, become more frequent, and last longer with climate change

To assess how heat stress will change in Southeast Asia, we examine three dimensions: intensity, frequency, and duration. Intensity (reflected here by daily maximum UTCI or WBGT) is important because it captures peak heat stress levels, which can be dangerous even if their occurrence is rare. Frequency addresses how often these peak thresholds are surpassed, indicating whether extreme conditions are becoming more common. Duration quantifies how long people are exposed to these extreme conditions – which is critical for understanding cumulative physiological strain and the viability of daily work–rest routines.

During the historical baseline, people in Southeast Asia experienced at least Very Strong Heat Stress 24.1% of the time (88 days per year), as measured by daily maximum UTCI (Fig. 1bi). Under RCP2.6, this frequency increases to 31.4–32.5% (115–119 days per year in far- and near-future respectively), and it rises further under RCP8.5 to 37.7–53.7% (138–196 days per year in near- and far-future respectively). The increase in daily maximum UTCI relative to the baseline (Fig. 1ai) is statistically significant across all scenarios (Mann–Whitney U test), with the 95th percentile increasing by 2.0°C by the near-future in RCP8.5 and 4.7°C by the far-future. The average daily duration in at least Very Strong Heat Stress each month also lengthens considerably (Fig. 1ci), from 0.5–3.0 h in the historical baseline to 0.8–3.6 h in RCP2.6 (near- and far-future), 1.1–4.4 h in near-future RCP8.5, and 2.1–6.4 h in far-future RCP8.5. Across all scenarios, April and May consistently record the longest daily durations at or above Very Strong Heat Stress.

WBGT captures the physiological impact of heat stress on a range of activities, including outdoor work. According to the WBGT results, it will become increasingly challenging to sustain heavier outdoor workloads as

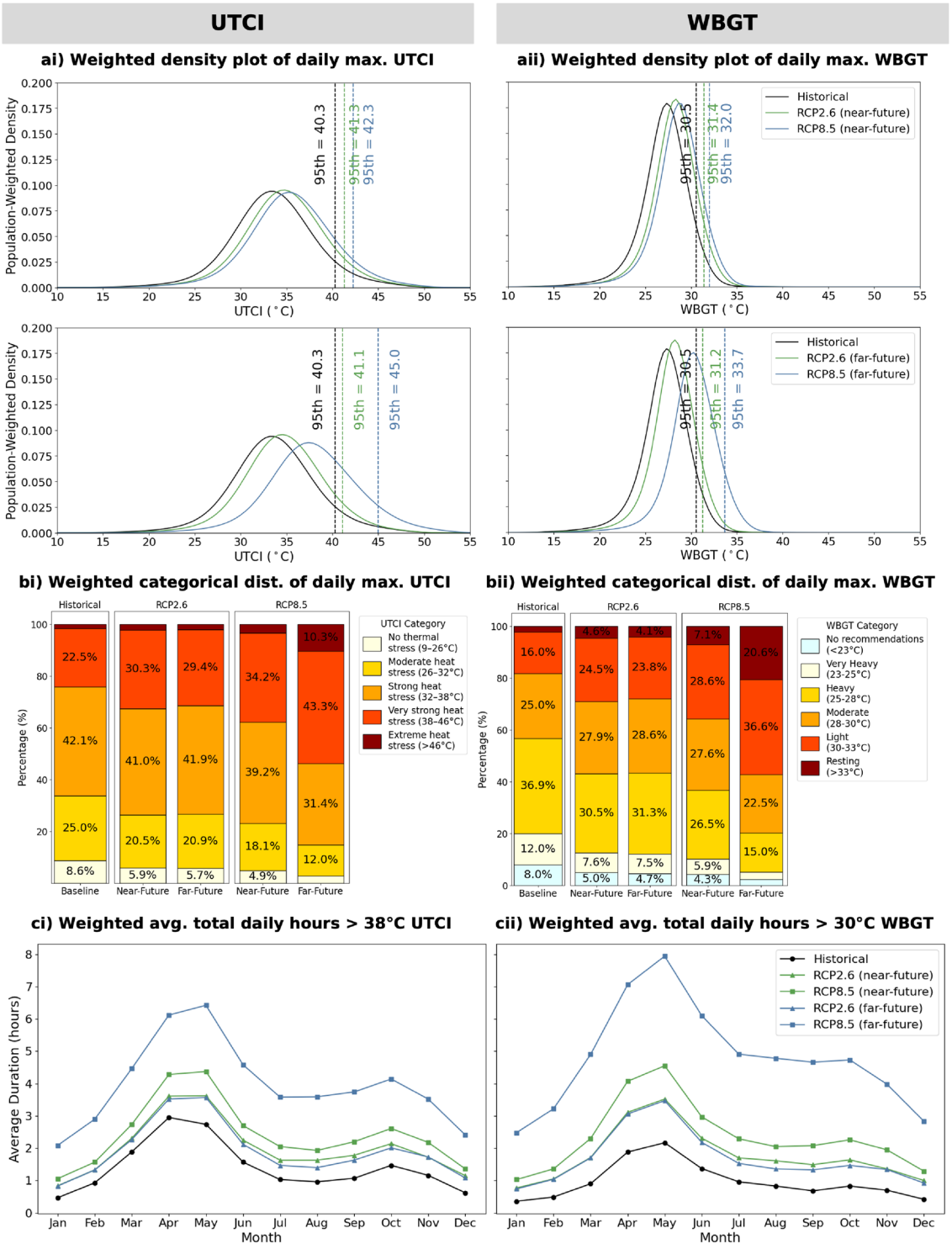

Fig. 1. Trends in the heat stress hazard due to climate change in Southeast Asia, as measured by UTCI and WBGT. (**a**) Density plot of maximum daily (i) UTCI and (ii) WBGT in the historical, near- and far- future periods under RCP 2.6 and RCP8.5, weighted according to population; (**b**) Annual distribution of heat stress categories, computed with the maximum daily (i) UTCI and (ii) WBGT in the historical, near- and far-future periods under RCP 2.6 and RCP8.5, weighted according to population; (**c**) Monthly average of total daily duration (hours) (i) > 38°C UTCI (Very Strong Heat Stress and above) and (ii) > 30°C WBGT (Light workloads and lower), weighted according to population, across all scenarios and time-periods considered.

the climate warms. Historically, maximum workloads were categorised as Light or lower 18.2% of the time (66 days per year); this increases to 27.2–29.1% in RCP2.6 (102–106 days in far- and near-future respectively) and 35.7–57.2% in RCP8.5 (130–209 days in near- and far-future respectively) (Fig. 1bii). As with the UTCI analysis, the most pronounced shifts appear under far-future RCP8.5, where Light workloads replace the Moderate workloads prevalent in the baseline, with the 95th percentile increasing by 3.2°C (Fig. 1aii), highlighting an intensification of peak WBGT levels. These increases in average daily maximum WBGT from the baseline to the near- and far-future periods are statistically significant in both RCP2.6 and RCP8.5 (Mann-Whitney *U* test). The average daily duration necessitating Light or lower workloads was 0.4–2.2 h in the baseline, increasing to 0.7–3.5 hours in RCP2.6 (near- and far-future), 1.0–4.6 hours in RCP8.5 (near-future), and 2.5–7.9 hours in RCP8.5 (far-future), again peaking in April and May across all scenarios (Fig. 1cii).

A greater proportion of people will be exposed to extreme levels of heat stress for more prolonged periods of time

Exposure to extreme heat stress increases across Southeast Asia in all scenarios and time periods considered (see Table 1). Extreme heat stress is defined as UTCI > 46°C and as WBGT > 33°C, corresponding to the highest categories of heat stress for each metric, and we focus the exposure analysis on these thresholds as they represent conditions where human thermoregulation is severely challenged and the health risks become critical. Exposure is quantified in person-hours, integrating the number of people exposed and the time they are exposed above a given threshold, thereby capturing the cumulative extent and persistence of extreme heat conditions. Even in the near-future, annual person-hours of exposure rise sharply: increasing by a factor of 2.8–4.6 as per UTCI and 4.6–7.9 as per WBGT (RCP2.6 vs. RCP8.5). The number of people experiencing seven or more consecutive days of extreme heat per year grows from 8.6 million in the baseline to 23.3–27.8 million in the near-future as per UTCI, and from 0.1 million to 6.6–16.9 million as per WBGT. Table S1 in Supplementary Information contains the exposure projections from individual driving GCM of the REMO RCM.

The increases in exposure are largely driven by changes in climate, as illustrated in Figs. 2b and 3b. To interpret the drivers of change, we decompose exposure into three components. The first is the climate effect, which represents the change in exposure solely due to shifts in climate conditions (e.g. increases in temperature). The second is the population effect, which reflects the change attributable to variations in the size or distribution of the population. The third is the interaction effect, which captures the residual component, reflecting non-linear or synergistic influences when climate change and population change occur simultaneously. For Southeast Asia, the climate effect is the main driver of increasing exposure. In the near-future, under RCP8.5 (Figs. 2bi and 3bi), climate accounts for 82% of total change in exposure as per UTCI and 73% with WBGT, with population (28% as per UTCI and 20% as per WBGT) and interaction (-10% as per UTCI and 7% as per WBGT) effects far lower. In the far-future, climate contributes even more to the increase in exposure (Figs. 2bii and 3bii), accounting for 88% (UTCI) and 97% (WBGT) of the increase across Southeast Asia. Climate remains the dominant contributor to the increase in exposure under RCP2.6 as well (see Figs. S1 and S2 in Supplementary Information). Conversely, the low population effect is largely driven by the threshold used to define extreme heat stress. Since the population effect holds climate constant at historical levels–and the threshold is rarely exceeded under historical conditions–the effect size remains relatively low. Moreover, the total population of Southeast Asia is higher in the near-future than far-future under both RCP2.6 and 8.5, which is in line with the assumptions made in these scenarios regarding decreasing fertility rates. As a result, exposure to extreme heat is lower in the far-future under RCP2.6, as population decreases and climate change is limited, but under RCP8.5, exposure increases as climate worsens to a larger degree than the reduction in population.

As seen in Figs. 2b and 3b, and Table S1 (Supplementary Information), the range in exposure projections across the model ensemble is notable. This spread reflects inter-model variability in the driving GCMs and the

	Extreme heat stress[1] indices	1976-2005	2030-2059		2070-2099	
		Baseline	RCP2.6	RCP8.5	RCP2.6	RCP8.5
UTCI	Weighted avg. total annual hours in extreme heat	48.2	55.8	78.3	51.1	218.4
	Population exposed ≥ 3 days (millions)	21.3	55.7	71.4	43.0	161.7
	Population exposed ≥ 7 days (millions)	8.6	23.3	27.8	18.3	86.7
	Total annual person-hours exposure (billions)	8.3	23.5	38.3	17.2	109.5
WBGT	Weighted avg. total annual hours in extreme heat	29.9	68.7	116.8	61.8	439.0
	Population exposed ≥ 3 days (millions)	13.9	110.9	147.1	81.3	311.7
	Population exposed ≥ 7 days (millions)	0.1	6.6	16.9	4.6	160.8
	Total annual person-hours exposure (billions)	9.9	45.5	77.9	33.9	241.7

Table 1. Metrics of annual exposure to extreme heat stress, computed with UTCI and WBGT, representing the mean exposure across the ensemble. [1]Extreme heat stress is defined as UTCI > 46°C and as WBGT > 33°C

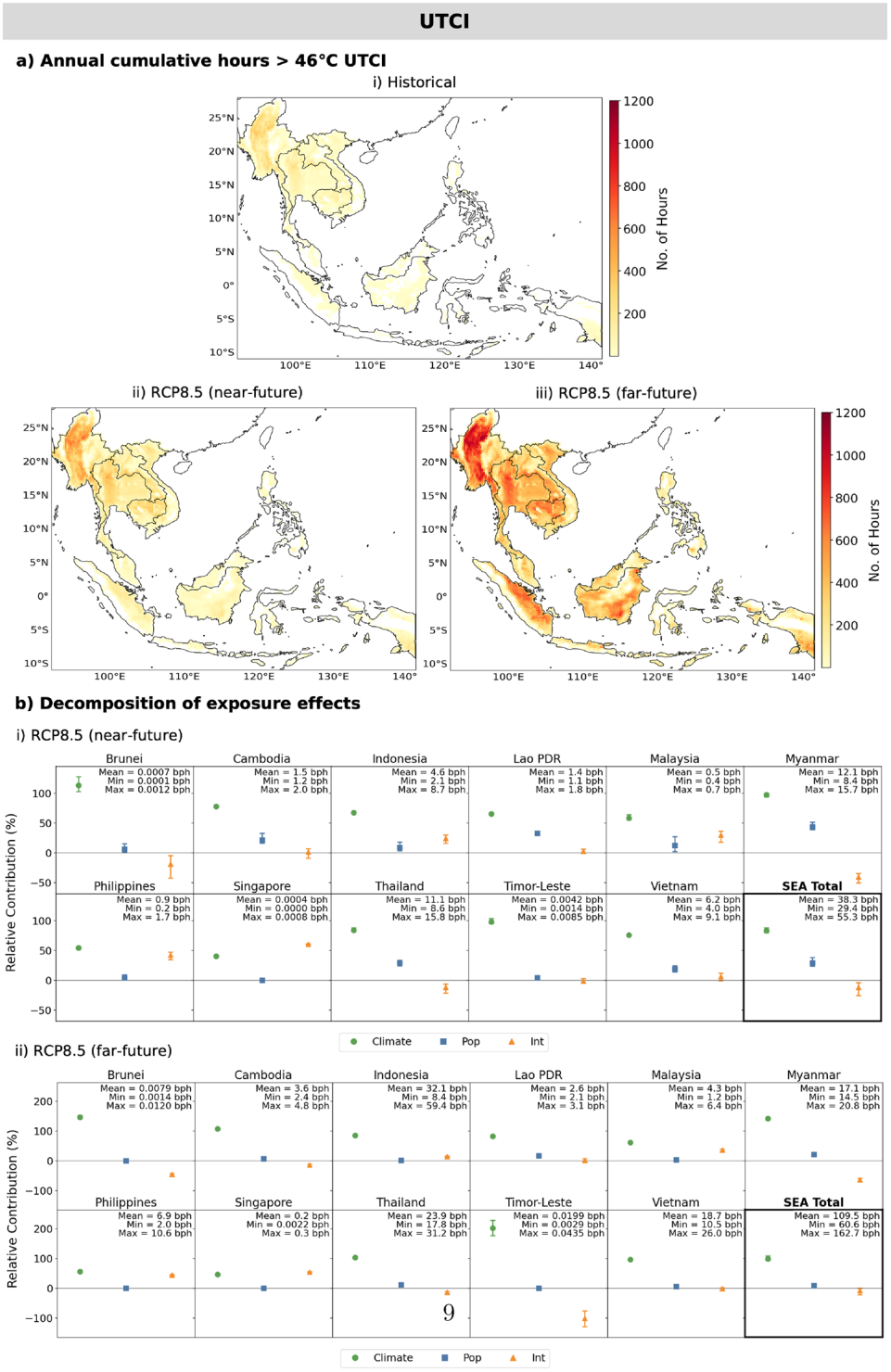

Fig. 2. Exposure to extreme heat stress in Southeast Asia, as computed by UTCI for RCP8.5. (**a**) Maps of annual cumulative hours > 46°C UTCI (Extreme Heat Stress) in the (i) historical, (ii) near-future and (iii) far-future time periods; (**b**) Decomposition of the relative contribution of climate, population and interaction effects to total person-hours exposure to > 46°C UTCI (Extreme Heat Stress) in the (i) near-future (ii) far-future time periods, for Southeast Asia as a whole and each country. Symbols show the ensemble mean of the REMO RCM; whiskers indicate the min–max range. Panel annotations also report the mean and range of total exposure in billion person-hours (bph) across the ensemble. Maps created in Python (v3.12.4) using Matplotlib (v3.9.0) and Cartopy (v0.23.0). Coastlines and borders from Natural Earth (public domain).

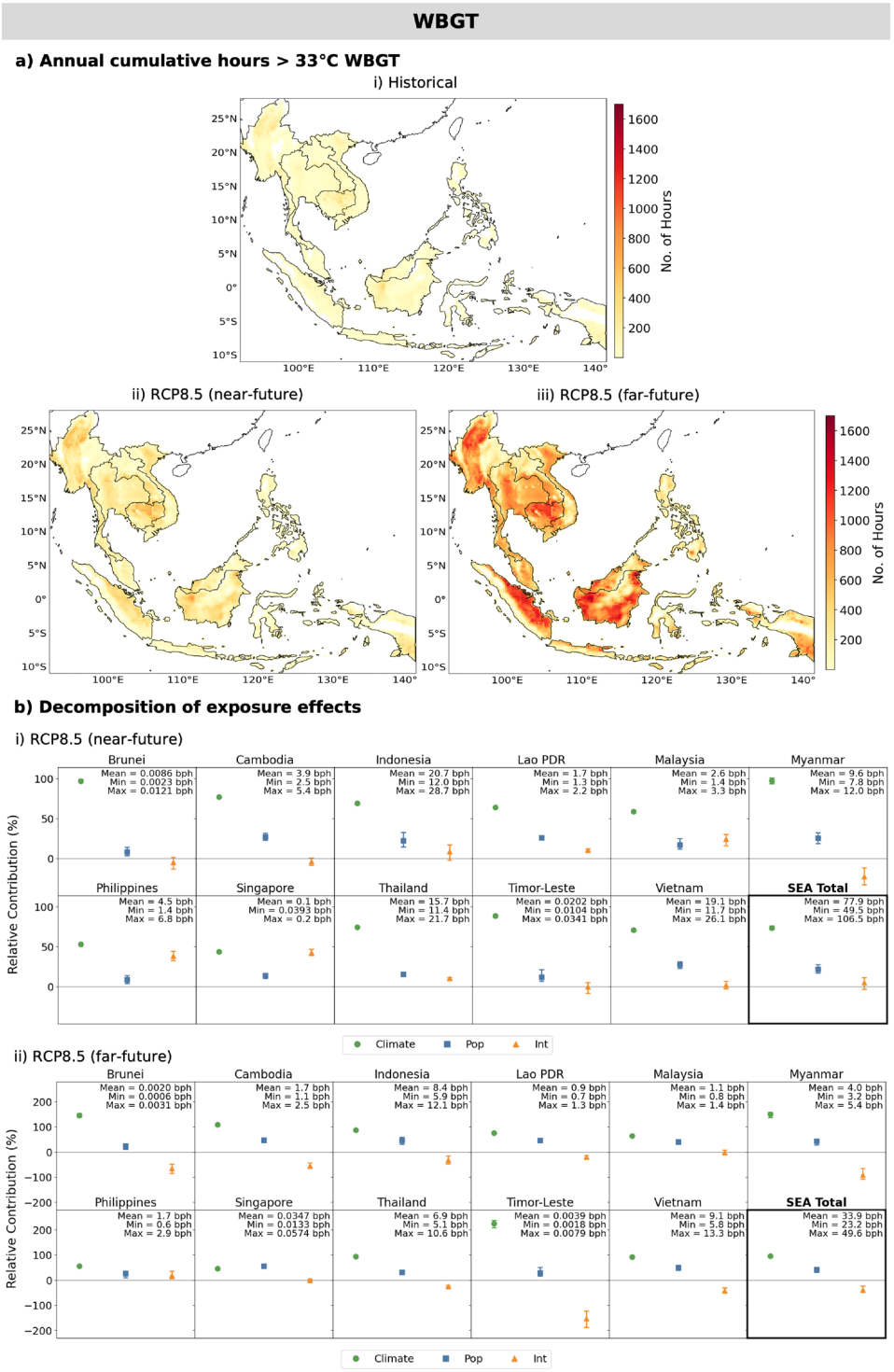

Fig. 3. Exposure to extreme heat stress in Southeast Asia, as computed by WBGT for RCP8.5. (**a**) Maps of annual cumulative hours > 33°C WBGT (Resting workload) in the (i) historical, (ii) near-future and (iii) far-future time periods; (**b**) Decomposition of the relative contribution of climate, population and interaction effects to total person-hours exposure to > 33°C WBGT (Resting workload) in the (i) near-future (ii) far-future time periods, for Southeast Asia as a whole and each country. Symbols show the ensemble mean of the REMO RCM; whiskers indicate the min–max range. Panel annotations also report the mean and range of total exposure in billion person-hours (bph) across the ensemble. Maps created in Python (v3.12.4) using Matplotlib (v3.9.0) and Cartopy (v0.23.0). Coastlines and borders from Natural Earth (public domain).

sensitivity of extreme-value estimates to the selected thresholds (UTCI > 46°C, WBGT > 33°C). However, all models consistently indicate a strong increase in exposure across both RCPs, and even the most conservative models show substantial increases in exposure. For example, in RCP8.5 (near-future), exposure to extreme UTCI increases by 435% (MPI-M-MPI-ESM-LR) and exposure to extreme WBGT increases by 460% (NCC-NorESM1-M) - see Table S1 for more details. This suggests that the overall trend is robust despite model-to-model differences.

Broken down by countries, exposure to extreme UTCI is highest in Myanmar, Thailand and Vietnam in the near-future, but by the far-future, exposure becomes the greatest in Indonesia. Exposure to extreme WBGT is greatest in Indonesia, Vietnam and Thailand in both the near-future and far-future. In these countries and others in Southeast Asia, climate is the main effect driving the increases in exposure, as measured by both UTCI and WBGT. Some countries, such as Brunei, Myanmar, Thailand and Timor-Leste, have negative interaction effects, and this is likely due to climate worsening in places where population is decreasing relative to the baseline.

Heat stress will be most severe in continental Southeast Asia

Continental Southeast Asia, located in the northwestern part of the region, exhibits the highest monthly average heat stress based on daily maximum UTCI and WBGT values (Figs. 4 and 5). Peak heat stress occurs from March to May, coinciding with the continental summer. These regions also experience the longest daily duration of severe heat exposure, with approximately 6–9 h per day classified as Very Strong Heat Stress or higher (UTCI) or permitting only Light or lower workloads (WBGT) during the summer months in the near-future and increasing to 10–12 h per day in the far-future. These spatial patterns are consistent in RCP2.6 as well (see Figs. S3–S6 in Supplementary Information).

Although less extreme than the continental region, Indonesia also experiences elevated heat stress, with September–November monthly averages reaching Strong Heat Stress (UTCI) and Moderate workload limits (WBGT) in the near-future, and Very Strong Heat Stress (UTCI) and Light workload limits in the far-future (WBGT). Malaysia and Singapore experience consistently high heat stress levels year-round, with monthly averages frequently at or near Strong Heat Stress (UTCI) and Moderate workload thresholds (WBGT) for most of the year in the near-future, and Very Strong Heat Stress (UTCI) and Light workload thresholds (WBGT) in the far-future.

Discussion

Our findings extend upon earlier regional studies which demonstrated that heatwaves in Southeast Asia would become more extreme and frequent with climate change, based on temperature indices[1,11–13]. While these studies illustrate there will be increasing risk from extreme heatwaves in a warming climate, the use of bioclimatic indices in this study help to contextualise the impacts on health and labour productivity. As highlighted in the results, the higher thresholds of UTCI (Very Strong and Extreme Heat Stress) and WBGT (Light and Resting workloads) will become more frequent, posing challenges to human physiological adaptability in the region and increasing the risk of heat-related illnesses. At UTCI levels > 38°C (Very Strong Heat Stress), the human body experiences severe thermoregulatory strain - core temperature rises precipitously, sweat mechanisms become inefficient, and cardiovascular systems are pushed to their limits, which increase risks of heat exhaustion, stroke, and cardiovascular mortality[24,27]. When UTCI surpasses 46°C (Extreme Heat Stress), even healthy individuals become vulnerable to life-threatening hyperthermia within hours of exposure[24,27]. The parallel WBGT findings have equally severe implications for labour: at WBGT $>$ 30°C (Light workload), workers must take frequent, prolonged breaks to avoid cumulative heat strain, while conditions $>$ 33°C (Resting workload) indicate an environment where even minimal physical activity can lead to dangerous levels of heat strain, severely limiting labour capacity and posing serious health risks[15,28]. The results also demonstrate that heat stress will already increase in the near-future, with an additional 20–50 days per year in Very Strong Heat Stress (UTCI) and 30–60 days in Light workloads (WBGT), highlighting the urgent need for countries to prepare their communities, infrastructure, healthcare systems and economies for heightened levels of heat stress. While countries across Southeast Asia have made varying progress in heat adaptation – through sectoral guidelines, early-warning systems, and community outreach – none have yet implemented a comprehensive national heat action plan. Such a plan is critical for coordinating timely heat–health responses, protecting vulnerable populations, minimising labour disruptions, and strengthening institutional preparedness amid escalating heat stress[29].

With the high temporal resolution used in this study, we are able to quantify not only the frequency but also the specific hours per day during which extreme heat stress occurs, providing actionable insights for adaptation strategies. For example, our results show that in the far-future RCP8.5 scenario, populations across Southeast Asia will endure $\geq$ 6 hours/day of 'Very Strong Heat Stress' or worse on average, far exceeding thresholds for safe outdoor activity. In high-risk countries (Myanmar, Cambodia, Thailand), the summer months will bring 10–12 h/day where only 'Light' or 'Resting' work is advisable, drastically reducing productive outdoor labour. The projected increase in the duration of hazardous conditions highlights the need for policymakers and employers to use these high-resolution projections to design more effective work–rest schedules and to allocate cooling resources strategically during critical periods. Additionally, these high-resolution data enable the development of early-warning systems that target the specific periods when heat stress intensity and duration peak, thereby allowing for timely public health advisories and operational adjustments. At present, there is a large disparity in the level of preparedness to tackle extreme heat among countries in Southeast Asia[22]. While some countries, such as Singapore, Thailand and Vietnam, have workplace regulations in terms of heat stress guidelines[30], others including Indonesia, Myanmar, Cambodia, Lao PDR, and Timor-Leste, have little to no early warning systems to alert the public on heatwaves and issue health advisories. However, as seen in the results, many countries lacking heat-advisory systems are also those facing the highest levels and longest durations of heat stress, particularly during the summer months. By providing granular information on the hours of extreme heat exposure, our

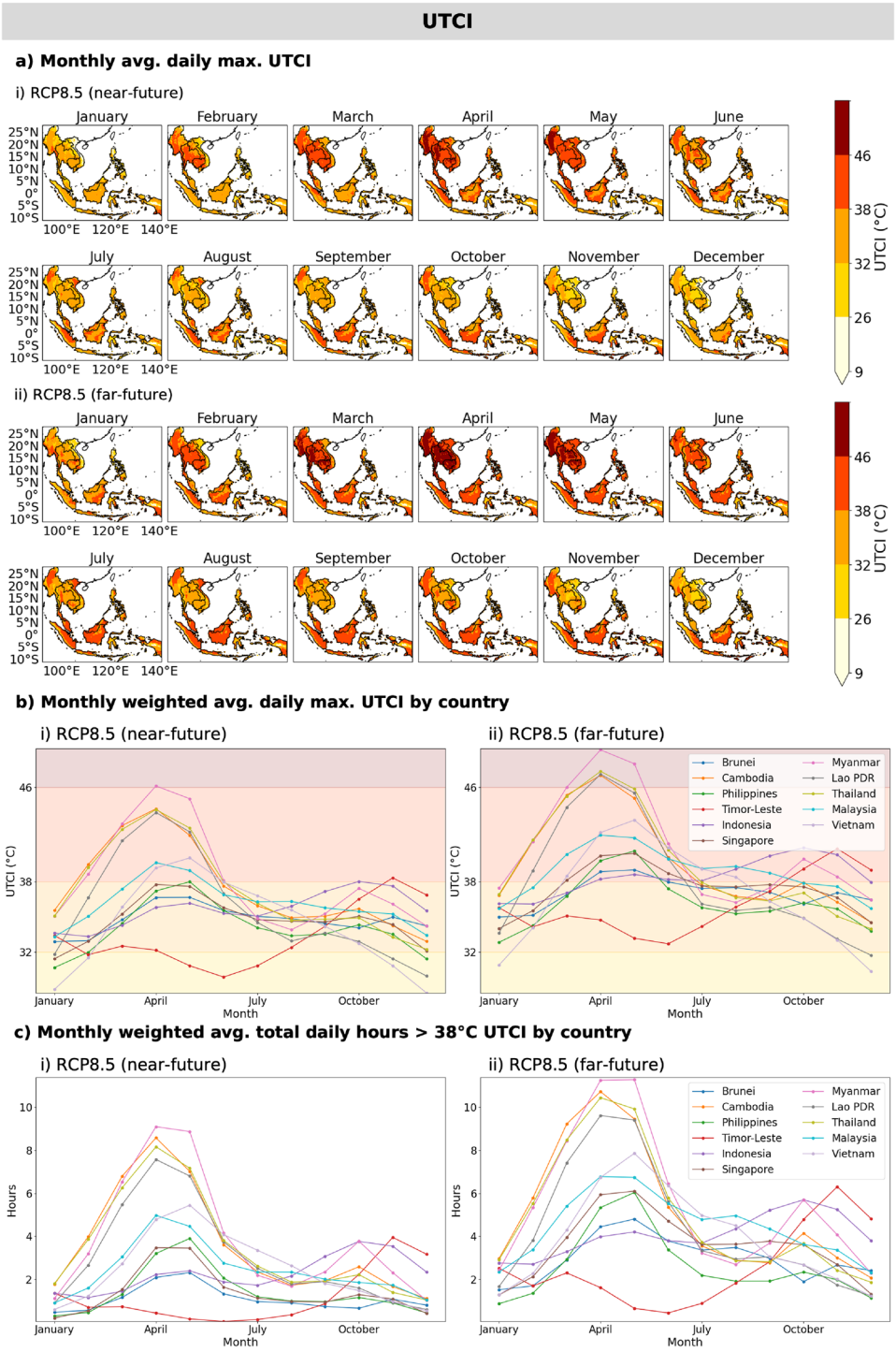

Fig. 4. Spatial patterns of heat stress in Southeast Asia, as computed by UTCI for RCP8.5. (**a**) Maps of monthly average daily maximum UTCI in the (i) near-future and (ii) far-future; (**b**) Line plots of monthly average daily maximum UTCI, weighted by population, for each country in the (i) near-future and (ii) far-future; (**c**) Line plots of monthly average total daily hours > 38°C UTCI (i) (Very Strong Heat Stress), weighted by population, for each country in the (i) near-future and (ii) far-future. Maps created in Python (v3.12.4) using Matplotlib (v3.9.0) and Cartopy (v0.23.0).

findings offer a crucial basis for these less-prepared regions to enhance their climate resilience measures and better protect vulnerable populations from the escalating risks of heat-related illnesses and labour disruptions.

Our analysis suggests that escalating exposure to extreme heat stress is primarily driven by climate, specifically increases in thermal stress arising solely from shifts in temperature, humidity, wind, and radiation patterns. In other words, climate accounts for the majority of the rise in person-hours of exposure, as demonstrated by

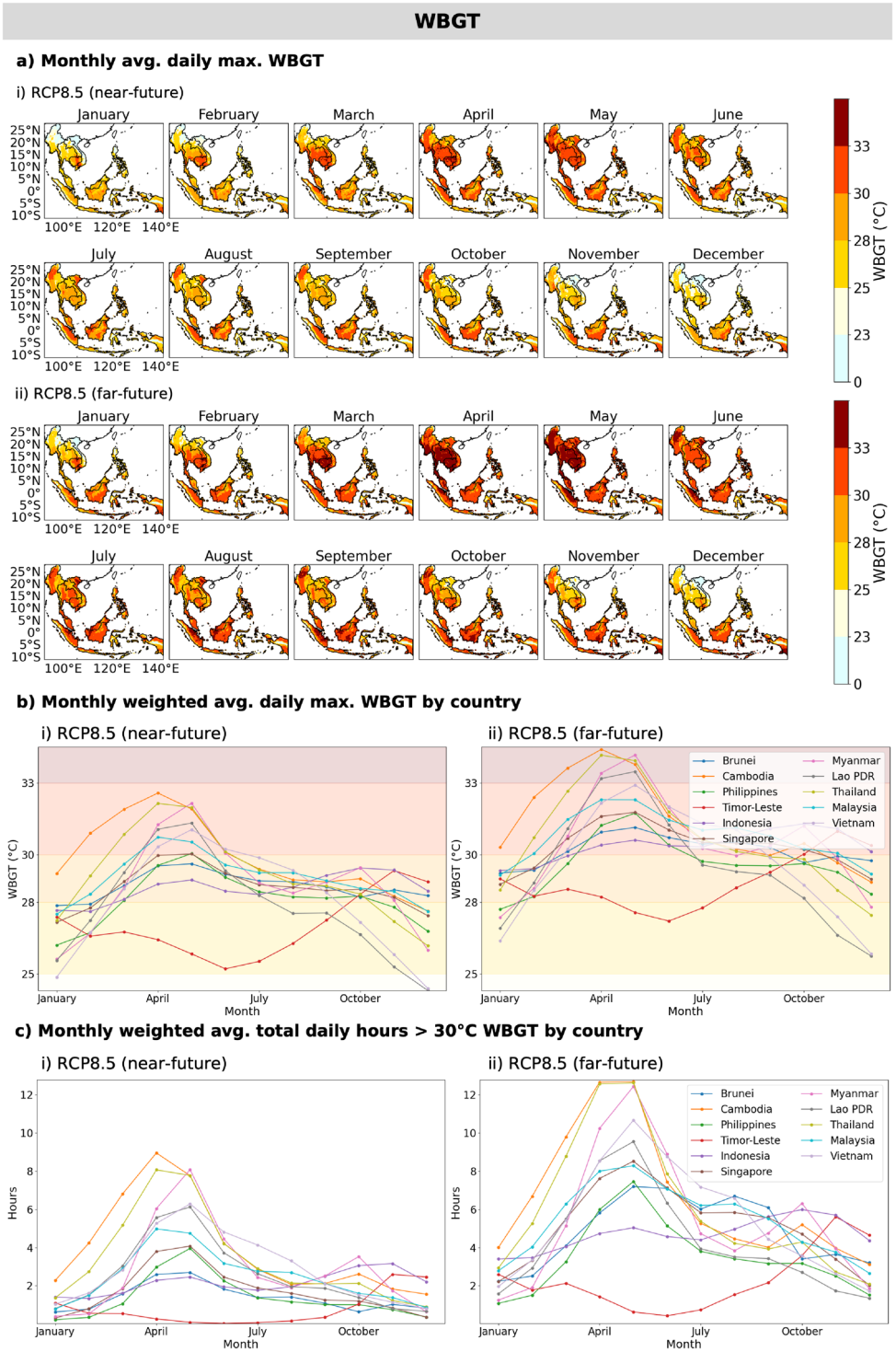

Fig. 5. Spatial patterns of heat stress in Southeast Asia, as computed by WBGT for RCP8.5. (**a**) Maps of monthly average daily maximum WBGT in the (i) near-future and (ii) far-future; (**b**) Line plots of monthly average daily maximum WBGT, weighted by population, for each country in the (i) near-future and (ii) far-future; (**c**) Line plots of monthly average total daily hours > 30°C WBGT (Light workload), weighted by population, for each country in the (i) near-future and (ii) far-future. Maps created in Python (v3.12.4) using Matplotlib (v3.9.0) and Cartopy (v0.23.0). Coastlines and borders from Natural Earth (public domain).

the marked differences between future climate scenarios. In contrast, the changes in the number and spatial distribution of people contributes relatively modestly to the overall increase. The interaction effect, representing the non-linear and synergistic influences when climate change and population shifts occur simultaneously, amplifies exposure only in specific regions where growing populations coincide with rapidly worsening climate

conditions. This finding differs from Ref. 11 who found that interaction effects are greatest in driving exposure to warm days in Southeast Asia, but more aligned with[12] who found that in terms of exposure to compound heatwaves, climate effects are strongest for younger age cohorts but interactions effects dominate for older age cohorts. The difference may arise from the use of relative thresholds in Refs. 11 and 12 based on historical baselines (e.g. the 90th percentile of daily maximum temperature), which might moderate the apparent increase in exceedance under future climates, whereas our use of absolute thresholds (UTCI $> 46^{\circ}$C and WBGT $> 33^{\circ}$C) might exhibit a much sharper rise in exceedance under warming scenarios. Our results also indicate that the level of heat stress towards the end of the century is highly dependent on the climate scenario. Compared to far-future RCP2.6, exposure to extreme heat in far-future RCP8.5 scenario is approximately six times higher according to UTCI and seven times higher according to WBGT. These findings underscore that rapid and large-scale greenhouse gas mitigation measures are essential in curtailing the dominant climate effect, in order to reduce the overall exposure to extreme heat stress and prevent such conditions from becoming the new normal in the region.

There is notable inter-model spread in projected exposure to extreme heat stress. Exposure metrics based on exceedances of absolute thresholds (UTCI $> 46\,^{\circ}$C, WBGT $> 33\,^{\circ}$C) are highly sensitive to extreme value statistics, where small variations in simulated UTCI or WBGT near the upper tail can yield large differences in estimated exposure. This spread also reflects epistemic uncertainty arising from our incomplete knowledge of the climate system and its representation in models. The three driving GCMs differ in their climate sensitivities, feedback mechanisms, and parameterisations of sub-grid processes; HadGEM2-ES, for example, has a high equilibrium climate sensitivity and produces stronger warming, whereas MPI-ESM-LR and NorESM1-M exhibit lower climate sensitivities and generally project more moderate warming[31]. Such variability has critical implications for adaptation planning, as reliance on a single model could under- or over-estimate risk, whereas the ensemble captures a fuller range of plausible outcomes. The consistent, statistically significant increases in exposure across all models – including conservative estimates exceeding 400% – provide a high-confidence baseline for impacts, while the upper range highlights the potential for more severe outcomes. Our findings are consistent with other multi-model analyses of heat stress in Southeast Asia, which identify structural model differences as a dominant source of spread in projections of extreme heat (e.g. Refs. 11–13). Overall, despite the inter-model variability, the ensemble results point to a robust and consistent regional trend of increasing human exposure to extreme heat, with clear implications for public health and climate adaptation planning.

Methods

All analysis for this study were performed in Python (v3.12.4; https://www.python.org) using open-source libraries. Maps were created with Matplotlib (v3.9.0; https://matplotlib.org) and Cartopy (v0.23.0; https://cartopy.readthedocs.io). Coastlines and national borders were obtained from the Natural Earth dataset (public domain; https://www.naturalearthdata.com).

REMO RCM

The input data for this study were obtained from the REMO RCM[25,26], which is a hydrostatic atmospheric model that is part of the CORDEX-CORE initiative - a consistent, high-resolution climate dataset that provides downscaled climate projections for major land masses across the world[32]. The data for the Southeast Asia domain was available at a 22x22km resolution and 3-hourly time intervals. The variables needed to compute both UTCI and WBGT were air temperature (tas), relative humidity (hurs), wind speed (sfcWind) and surface radiation (rsus, rsds, rlus, rlds). Details on the model ensemble can be found in Table 2.

The REMO RCM used in this study is known to have low biases in Southeast Asia, with mean annual temperature bias within $\pm 0.5^{\circ}$C and mean annual precipitation bias typically below 10%[26]. While the overall bias in precipitation is low, the model's spatial standard deviation is relatively high (10-20%). This variability suggests that the projections may be less reliable in some regions. Additionally, while the 22×22 km resolution of the model offers improvements over coarser global models, it may still overlook fine-scale features such as urban heat islands and coastal effects. While multi-model ensembles reduce the uncertainty related to model biases, the advantage of the current dataset is its superior spatial and temporal resolution that allows for the calculation of diurnal heat metrics at high spatial resolutions.

Bias analysis comparing the RCM results with ERA-Interim reanalysis data showed that UTCI on average has a bias of -1.23°C and WBGT has a bias of -0.88°C (see Fig. S7ai and bi in Supplementary Information). We also computed this for daily maxima, with an average bias of -1.59°C (daily max. UTCI) and -1.11°C (daily max. WBGT) (see Fig. S7aii and bii in Supplementary Information). These small negative biases suggest that the RCM may slightly underestimate heat stress, consistent with the cold temperature bias reported for REMO in parts of Southeast Asia[26]. Given that the magnitude of the bias is low, we did not apply additional bias correction. This bias does not affect the projected changes we report, as it is present in both the baseline and future periods.

Global climate model	Realisation	Regional climate model	Scenarios
MPI-M-MPI-ESM-LR	r1i1p1	GERICS-REMO2015	Historical, RCP2.6, RCP8.5
MOHC-HadGEM2-ES	r1i1p1		
NCC-NorESM1-M	r1i1p1		

Table 2. Details of the REMO model data used in this study.

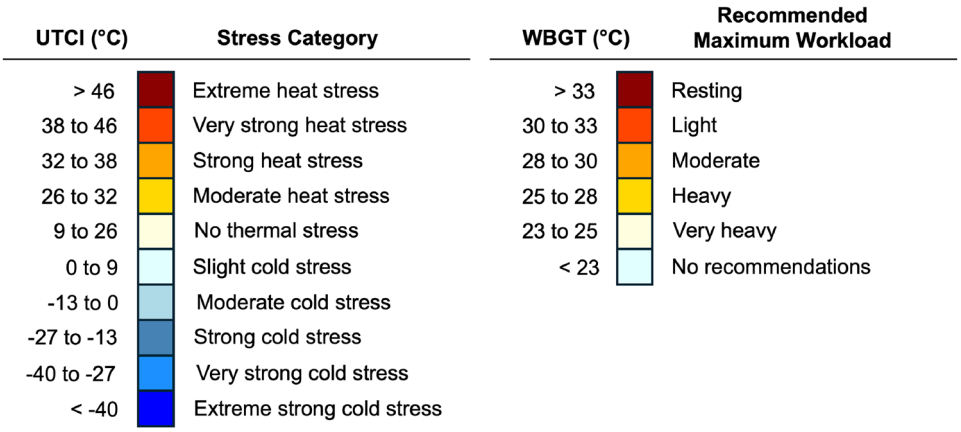

Fig. 6. Graphic of UTCI categories, defined by thermal stress, and WBGT categories, defined by the recommended maximum workload, with corresponding temperature ranges.

UTCI & WBGT

UTCI is represented by Eq. (1), and expresses the air temperature (T_a) in the reference condition, which causes the same modeled physiological response – as predicted by the UTCI-Fiala model[33] – as that produced by the actual environmental conditions[24]. The reference conditions in the model assume an individual walking outdoors at 4km/h, with a metabolic heat production rate of 2.3 MET ($\cong 135\ W/m^2$), in an environment with a wind speed (v_a) of $\cong$ 0.5m/s at 10m height, a mean radiant temperature (T_r) that's equal to T_a, and relative humidity (p_a) of 50% (at $T_a > 29^{\circ}$C the reference humidity was taken to be constant at 20 hPa)[24]. UTCI is expressed as 10 categories of thermal stress, which correspond to specific physiological responses (see[24] for details). The UTCI computations for this study were performed with the open-source *xclim* python library[34], through the *index_calculator* wrapper developed at GERICS to streamline calculation of climate indicators from CMORized NetCDF files[35].

$$\mathrm{UTCI}(T_a, T_r, v_a, p_a) = T_a + \mathrm{Offset}(T_a, T_r, v_a, p_a), \tag{1}$$

where

$$\begin{aligned} T_a &= \text{ air temperature} \\ T_r &= \text{ mean radiant temperature} \\ v_a &= \text{ wind speed at 10m} \\ p_a &= \text{ humidity, expressed as water vapour pressure} \end{aligned}$$

WBGT is represented by Eq. (2), which is a weighted average of the natural wet bulb temperature (T_w), globe temperature (T_g) and dry-bulb temperature (T_a)[36]. T_g represents the environmental heat load, T_w represents the ease of evaporation (or lack thereof), and T_a represents the additional heat load from being outdoors[36]. We adopted the variation proposed by[37], whereby mean radiant temperature is used to calculate the globe temperature, as it more accurately approximates the effect of radiation on heat stress. The computations of WBGT in this study were performed with the open-source *thermofeel* python library[38].

$$\mathrm{WBGT} = 0.7T_w + 0.2T_g + 0.1T_a, \tag{2}$$

where

$$\begin{aligned} T_w &= \text{ natural wet bulb thermometer temperature}(^{\circ}\text{ C}) \\ T_g &= \text{ globe thermometer temperature}(^{\circ}\text{C}) \\ T_a &= \text{ 2 m air temperature, or dry-bulb temperature}(^{\circ}\text{ C}) \end{aligned}$$

The outputs for both UTCI and WBGT were obtained at a 22x22km resolution for the historical (1976-2005), near-future (2030-2059) and far-future (2070-2099) time periods at 3-hourly intervals. The analyses was performed on each of the individual driving GCMs of the REMO RCM, as well as the ensemble mean. The statistics reported in the main text are based on the ensemble mean, unless otherwise stated. The categorisations applied to the UTCI and WBGT metrics are found in Fig. 6.

The UTCI employs a standardised categorical scale consisting of ten distinct classes that range from extreme cold stress to extreme heat stress. Each category is defined by specific UTCI value intervals, which are linked to characteristic physiological responses to varying environmental conditions[24].The WBGT categories used in this study were obtained from[15,37], which establishes guidelines linking WBGT values to safe workload intensities. Under cooler conditions with lower WBGT readings, higher workloads (in terms of physical load)

can be sustained for longer periods, allowing for extended work durations and fewer rest breaks. Conversely, higher WBGT values and therefore higher heat stress, will require a reduction in the acceptable work load, shorter durations of continuous work, and longer or more frequent rest intervals to allow the body to recover and dissipate heat.

Exposure

Historical population data were obtained from the Global Human Settlement Layer dataset[39]. The data were obtained at 5-year intervals from 1975 onward at a 1x1km resolution, and resampled to 22x22km resolution to match that of the UTCI and WBGT outputs. Future population were obtained from downscaled SSP projections[40] for SSP1 and SSP5 (corresponding to RCP2.6 and RCP8.5) at 5-year intervals from 2030 onward at a 1x1km resolution and resampled to 22x22km. The population data were not only used in exposure computations, but also as weights in all averages computed. Since population projections were available only at 5-year intervals, and each population data point was assumed constant within its interval and matched to the corresponding climate data for that period.

To decompose the effects in exposure calculations we adopted the method by Ref. 41, which is represented by the following equation:

$$\Delta E = P_1 \times \Delta C + C_1 \times \Delta P + \Delta C \times \Delta P, \tag{3}$$

where

ΔE is the total change in population exposure to heat extremes.
P_1 is the baseline population.
ΔC is the change in heat extremes relative to the baseline.
C_1 is the baseline level of heat extremes.
ΔP is the change in population relative to the baseline.

To separate the drivers of exposure change, we calculated the contributions from climate, population, and their interaction. The climate effect represents how much exposure changes when only the level of heat stress changes, holding population fixed at the baseline. The population effect represents how much exposure changes when only population changes, holding climate fixed at the baseline. The interaction effect captures the combined influence when both climate and population change at the same time.

These components were computed at the grid-cell level and then summed to obtain regional totals. To compare their relative importance, we expressed each component as a percentage of the total change in exposure. By construction, the three components always sum to 100%. The contributions are reported as signed values, which means they can be either positive or negative. The interaction is positive when population growth coincides with areas experiencing stronger increases in heat stress, amplifying overall exposure. Conversely, the interaction is negative when population growth is concentrated in areas where heat stress decreases or remains stable, or when population declines occur in areas where heat extremes intensify. In such cases, the combined effect of climate and population dampens rather than amplifies exposure.

Data availability

The UTCI and WBGT results computed in this study are partially available at https://doi.org/10.5281/zenodo.17020558 and the full dataset can be requested from the lead author (Sonali Manimaran, emsonali@gmail.com). REMO RCM data are partially available through https://esgf-metagrid.cloud.dkrz.de/, and the full dataset can be requested from the Climate Service Centre Germany (GERICS). The historical population data can be accessed through https://human-settlement.emergency.copernicus.eu/download.php, and future population data through https://figshare.com/articles/dataset/Projecting_1_km-grid_population_distributions_from_2020_to_2100_globally_under_shared_socioeconomic_pathways/19608594/2.

Received: 4 July 2025; Accepted: 12 November 2025
Published online: 29 December 2025

References

1. Dong, Z. et al. Heatwaves in Southeast Asia and their changes in a warmer world. *Earth's Future* **9**(7), e2021EF001992. https://doi.org/10.1029/2021EF001992 (2021).
2. Fan, Y., Li, J., Zhu, S., Li, H. & Zhou, B. Trends and variabilities of precipitation and temperature extremes over Southeast Asia during 1981–2017. *Meteorol. Atmos. Phys.* **134**(4), 78. https://doi.org/10.1007/s00703-022-00913-6 (2022).
3. Li, X.-X. Heat wave trends in Southeast Asia during 1979–2018: The impact of humidity. *Sci. Total Environ.* **721**, 137664. https://doi.org/10.1016/j.scitotenv.2020.137664 (2020).
4. Rogers, C. D. W. et al. Recent increases in exposure to extreme humid-heat events disproportionately affect populated regions. *Geophys. Res. Lett.* **48**(19), 2021–094183. https://doi.org/10.1029/2021GL094183 (2021).
5. Thirumalai, K., DiNezio, P. N., Okumura, Y. & Deser, C. Extreme temperatures in Southeast Asia caused by El Niño and worsened by global warming. *Nat. Commun.* **8**(1), 15531. https://doi.org/10.1038/ncomms15531 (2017).
6. CNN: Southeast Asia Heatwaves: Education and School Closures. https://edition.cnn.com/2024/05/09/asia/southeast-asia-heatwaves-education-school-closures-intl-hnk/index.html (2024).
7. The Guardian: Inside an Oven: How Life in South-East Asia Is a Struggle Amid Sweltering Heat. https://www.theguardian.com/environment/article/2024/may/04/inside-an-oven-how-life-in-south-east-asia-is-a-struggle-amid-sweltering-heat (2024).

8. South China Morning Post: Southeast Asia's Brutal Heatwave: Daily Life and Agriculture Endangered by Rising Temperatures. https://www.scmp.com/week-asia/health-environment/article/3261584/southeast-asias-brutal-heatwave-daily-life-and-agriculture-endangered-rising-temperatures (2024).
9. United Nations, Department of Economic and Social Affairs, Population Division: World population prospects 2024: Summary of results. Technical Report UN DESA/POP/2024/TR/NO.9, United Nations, New York. https://desapublications.un.org/publications/world-population-prospects-2024-summary-results (2024).
10. Dahiya, B. Southeast Asia and sustainable urbanization. *Global Asia* **9**(3), 84–91 (2014).
11. Sun, X., Ge, F., Fan, Y., Zhu, S. & Chen, Q. Will population exposure to heat extremes intensify over Southeast Asia in a warmer world?. *Environ. Res. Lett.* **17**(4), 044006. https://doi.org/10.1088/1748-9326/ac48b6 (2022).
12. Sun, X., Ge, F., Chen, Q., Fraedrich, K. & Li, X. How striking is the intergenerational difference in exposure to compound heatwaves over Southeast Asia?. *Earth's Future* **11**(6), 2022–003179. https://doi.org/10.1029/2022EF003179 (2023).
13. Zhu, S. et al. Conspicuous temperature extremes over Southeast Asia: seasonal variations under $1.5\,^{\circ}$C and $2\,^{\circ}$C global warming. *Clim. Change* **160**(3), 343–360. https://doi.org/10.1007/s10584-019-02640-1 (2020).
14. Jendritzky, G., De Dear, R. & Havenith, G. UTCI-why another thermal index?. *Int. J. Biometeorol.* **56**(3), 421–428. https://doi.org/10.1007/s00484-011-0513-7 (2012).
15. International Organization for Standardization: Ergonomics of the thermal environment – assessment of heat stress using the WBGT (wet bulb globe temperature) index. Technical Report ISO 7243:2017, International Organization for Standardization, Geneva. https://www.iso.org/standard/67188.html (2017).
16. Wong, M. C., Wang, J., Zhi, X. & Dong, L. A 1940–2020 spatiotemporal analysis of thermal discomfort days in Southeast Asian countries. *Environ. Res. Commun.* **6**(10), 101009. https://doi.org/10.1088/2515-7620/ad810b (2024).
17. Kjellstrom, T., Lemke, B. & Otto, M. Mapping occupational heat exposure and effects in South-East Asia: Ongoing time trends 1980–2011 and future estimates to 2050. *Ind. Health* **51**(1), 56–67. https://doi.org/10.2486/indhealth.2012-0174 (2013).
18. Liu, Z. et al. Global and regional changes in exposure to extreme heat and the relative contributions of climate and population change. *Sci. Rep.* **7**, 43909. https://doi.org/10.1038/srep43909 (2017).
19. Chen, J. et al. Global socioeconomic exposure of heat extremes under climate change. *J. Clean. Prod.* **277**, 123275. https://doi.org/10.1016/j.jclepro.2020.123275 (2020).
20. Freychet, N. et al. Robust increase in population exposure to heat stress with increasing global warming. *Environ. Res. Lett.* **17**(6), 064049. https://doi.org/10.1088/1748-9326/ac71b9 (2022).
21. Li, D., Yuan, J. & Kopp, R. E. Escalating global exposure to compound heat-humidity extremes with warming. *Environ. Res. Lett.* **15**(6), 064003. https://doi.org/10.1088/1748-9326/ab7d04 (2020).
22. ASEAN Secretariat: ASEAN state of climate change report: Current status and outlook of the ASEAN region toward the ASEAN Climate Vision 2050. Technical report, ASEAN Secretariat, Jakarta. https://asean.org/wp-content/uploads/2021/10/ASCCR-e-publication-Correction_8-June.pdf (2021).
23. Kakaei, H., Omidi, F., Ghasemi, R., Sabet, M. R. & Golbabaei, F. Changes of WBGT as a heat stress index over the time: A systematic review and meta-analysis. *Urban Clim.* **27**, 284–292. https://doi.org/10.1016/j.uclim.2018.12.009 (2019).
24. Błażejczyk, K. et al. An introduction to the universal thermal climate index (UTCI). *Geogr. Pol.* **86**(1), 5–10. https://doi.org/10.7163/GPol.2013.1 (2013).
25. Jacob, D. et al. Assessing the transferability of the regional climate model REMO to different COordinated regional climate downscaling EXperiment (CORDEX) regions. *Atmosphere* **3**(1), 181–199. https://doi.org/10.3390/atmos3010181 (2012).
26. Remedio, A. R. et al. Evaluation of new CORDEX simulations using an updated Köppen-Trewartha climate classification. *Atmosphere* **10**(11), 726. https://doi.org/10.3390/atmos10110726 (2019).
27. Romaszko, J., Dragańska, E., Jalali, R., Cymes, I. & Glińska-Lewczuk, K. Universal climate thermal index as a prognostic tool in medical science in the context of climate change: A systematic review. *Sci. Total Environ.* **828**, 154492. https://doi.org/10.1016/j.scitotenv.2022.154492 (2022).
28. Kjellstrom, T. et al. Heat, human performance, and occupational health: A key issue for the assessment of global climate change impacts. *Annu. Rev. Public Health* **37**, 97–112. https://doi.org/10.1146/annurev-publhealth-032315-021740 (2016).
29. Hess, J. J. et al. Public health preparedness for extreme heat events. *Annu. Rev. Public Health* **44**, 301–321. https://doi.org/10.1146/annurev-publhealth-071421-025508 (2023).
30. Flouris, A., Azzi, M., Graczyk, H., Nafradi, B. & Scott, N. Heat at work: Implications for safety and health. Technical report, International Labour Organization, Geneva. A global review of the science, policy, and practice. https://www.ilo.org/publications/heat-work-implications-safety-and-health (2024).
31. Flato, G. et al. *Evaluation of Climate Models* 741–866 (Cambridge University Press, 2013). https://doi.org/10.1017/CBO9781107415324.020.
32. Gutowski, W. J. Jr. et al. WCRP COordinated regional downscaling EXperiment (CORDEX): A diagnostic MIP for CMIP6. *Geosci. Model Dev.* **9**(11), 4087–4095. https://doi.org/10.5194/gmd-9-4087-2016 (2016).
33. Fiala, D., Havenith, G., Bröde, P., Kampmann, B. & Jendritzky, G. UTCI-Fiala multi-node model of human heat transfer and temperature regulation. *Int. J. Biometeorol.* **56**(3), 429–441. https://doi.org/10.1007/s00484-011-0424-7 (2012).
34. Bourgault, P. et al. xclim: Xarray-based climate data analytics. *J. Open Source Softw.* **8**(85), 5415. https://doi.org/10.21105/joss.05415 (2023).
35. Buntemeyer, L., Lierhammer, L., Pfeifer, S., Buelow, K. & Manimaran, S. index_calculator: v0.11.0. Software. https://doi.org/10.5281/zenodo.10159231 (2023).
36. Minard, D. Prevention of heat casualties in marine corps recruits: Period of 1955–60, with comparative incidence rates and climatic heat stresses in other training categories. *Mil. Med.* **126**(4), 261–272 (1961).
37. Brimicombe, C. et al. Wet bulb globe temperature: Indicating extreme heat risk on a global grid. *GeoHealth* **7**(2), e2022GH000701. https://doi.org/10.1029/2022GH000701 (2023).
38. Brimicombe, C. et al. Thermofeel: A Python thermal comfort indices library. *SoftwareX* **18**, 101005. https://doi.org/10.1016/j.softx.2022.101005 (2022).
39. Schiavina, M., Freire, S., Carioli, A. & MacManus, K. GHS-POP R2023A - GHS population grid multitemporal (1975-2030). European Commission, Joint Research Centre (JRC). https://doi.org/10.2905/2FF68A52-5B5B-4A22-8F40-C41DA8332CFE . http://data.europa.eu/89h/2ff68a52-5b5b-4a22-8f40-c41da8332cfe (2023).
40. Wang, X., Meng, X. & Long, Y. Projecting 1 km-grid population distributions from 2020 to 2100 globally under shared socioeconomic pathways. *Sci. Data* **9**(1), 563. https://doi.org/10.1038/s41597-022-01675-x (2022).
41. Jones, B. et al. Future population exposure to us heat extremes. *Nat. Clim. Change* **5**, 652–655. https://doi.org/10.1038/nclimate2631 (2015).

Author contributions

S.M., D.W., C.N., L.B., and D.L. conceived and designed the study. S.M., D.W., C.N., and L.L. developed the methodology and software. S.M. performed the formal analysis and visualisation, and wrote the original draft. All authors contributed to the reviewing and editing of the manuscript. L.B. and D.L. supervised the project.

Funding
This work is supported by the following grants: the Helmholtz Information & Data Science Academy (HIDA) Visiting Researcher Grant to S.M.; the Ministry of Education, Singapore, under its MOE AcRF Tier 3 Award MOE2019-T3-1-004 to the Southeast Asia Sea-level (SEA2) Programme, supporting S.M., I.K., and D.L., and the MOE AcRF Tier 2 Award MOE-T2EP50222-0016, supporting D.W. and D.L.; and the Helmholtz Association under the programme "Changing Earth - Sustaining our Future", funding C.N., L.L., and L.B.

Declarations

Competing interests
The authors declare no competing interests.

Additional information
Supplementary Information The online version contains supplementary material available at https://doi.org/10.1038/s41598-025-28817-6.

Correspondence and requests for materials should be addressed to S.M.

Reprints and permissions information is available at www.nature.com/reprints.

Publisher's note Springer Nature remains neutral with regard to jurisdictional claims in published maps and institutional affiliations.